Searches for sterile neutrinos at the DANSS experiment

Mark Shirchenko[1,a] and *Nataliya* Skrobova[2,3,4,b]

[1] Joint Institute for Nuclear Research, Joliot-Curie 6, Dubna, Moscow region 141980, Russia
[2] Alikhanov Institute for Theoretical and Experimental Physics NRC "Kurchatov Institute", B. Cheremushkinskaya 25, Moscow 117218, Russia
[3] Lebedev Physical Institute of the Russian Academy of Sciences, 53 Leninskiy Prospekt, Moscow 119991, Russia
[4] Moscow Institute of Physics and Technology, 9 Institutskiy per., Dolgoprudny, Moscow Region 141701, Russia

Abstract. DANSS is a highly segmented 1 m^3 plastic scintillator detector. The DANSS detector is placed under an industrial 3.1 GW_{th} reactor of the Kalinin Nuclear Power Plant 350 km NW from Moscow. The distance to the core is varied on-line from 10.7 m to 12.7 m. The reactor building provides about 50 m water-equivalent shielding against the cosmic background. DANSS detects almost 5000 $\overline{\nu}_e$ per day at the closest position with the cosmic background less than 3%. The inverse beta decay process is used to detect $\overline{\nu}_e$. Sterile neutrinos are searched for assuming the 4ν model (3 active and 1 sterile ν). The exclusion area in the Δm^2_{14}, $\sin^2 2\theta_{14}$ plane is obtained using a ratio of positron energy spectra collected at different distances. Therefore results do not depend on the shape and normalization of the reactor $\overline{\nu}_e$ spectrum nor the detector efficiency. Results are based on 966 thousand antineutrino events collected at three different distances from the reactor core. The excluded area covers a wide range of the sterile neutrino parameters down to $\sin^2 2\theta_{14} < 0.01$ in the most sensitive region.

1. Introduction

The number of active neutrinos is limited to 3 by the measurements of the Z boson decay width [1]. However, the existence of additional sterile neutrinos is not excluded. Several effects [2,3] observed with about 3σ significance level can be explained by active-sterile neutrino oscillations [4]. Several experiments are searching now for sterile neutrinos [5–12].

The survival probability of a reactor $\overline{\nu}_e$ at short distances in the 4ν mixing scenario (3 active and 1 sterile neutrino) is described by an effective expression

$$1 - \sin^2 2\theta_{14} \sin^2 \left(\frac{1.27 \Delta m^2_{14}[\mathrm{eV}^2] L[\mathrm{m}]}{E_\nu[\mathrm{MeV}]} \right). \quad (1)$$

The existence of sterile neutrinos would manifest itself in distortions of the $\overline{\nu}_e$ energy spectrum at short distances. At longer distances these distortions are smeared out and the rate is reduced by a factor of $1 - \sin^2(2\theta_{14})/2$. Measurements at only one distance from a reactor core are not sufficient since the theoretical description of the $\overline{\nu}_e$ energy distribution is considered not to be reliable enough. The most reliable way to observe such distortions is to measure the $\overline{\nu}_e$ spectrum with the same detector at different distances. In this case, the shape and normalization of the $\overline{\nu}_e$ spectrum as well as the detector efficiency are canceled out. The DANSS experiment uses this strategy and measures $\overline{\nu}_e$ spectra at 3 distances from the reactor core centre: 10.7 m, 11.7 m, and 12.7 m to the detector centre. The detector positions are changed typically 3 times a week. Antineutrinos are detected by means of the Inverse Beta Decay (IBD) reaction

$$\overline{\nu}_e + p \rightarrow e^+ + n \text{ with } E_{\overline{\nu}} = E_{e^+} + 1.80\ \mathrm{MeV}. \quad (2)$$

2. The DANSS detector

The DANSS detector was constructed by the ITEP-JINR collaboration. It is installed under the core of a 3.1 GW_{th} industrial power reactor at the Kalinin Nuclear Power Plant (KNPP). The size of the reactor core is quite big: 3.7 m in height and 3.2 m in diameter. The reactor materials provide a good shielding equivalent to approximately 50 m of water, which removes the hadronic component of the cosmic background and reduces the cosmic muon flux by a factor of 6. DANSS consists of 2500 polystyrene-based scintillator strip ($1 \times 4 \times 100\,\mathrm{cm}^3$) with a thin Gd-containing surface coating. The coating serves as a light reflector and a (n, γ)-converter simultaneously. The detector is placed inside a composite shielding of copper, borated polyethylene and lead. It is surrounded on 5 sides (excluding bottom) by double layers scintillator plates to veto cosmic muons. Light from the strip is collected with three wavelength-shifting (WLS) fibers, glued into grooves along the strip. The central fiber is read out with a Silicon PhotMultiplier (SiPM). The side fibers from 50 parallel strips (a module – 10 layers with 5 strips each) are read out with a compact photomultiplier tube (PMT), so that the whole detector (2500 strips) is a structure of 50 intercrossing modules. SiPMs (PMTs) register about 18 (20) photo-electrons (p.e.) per MeV. These numbers were obtained using measurements with cosmic muons. So the total number is 38 p.e./MeV. Parameterized strip response non-uniformities have been incorporated into the

[a] e-mail: mark.shirchenko@jinr.ru
[b] e-mail: nataliya.skrobova@gmail.com

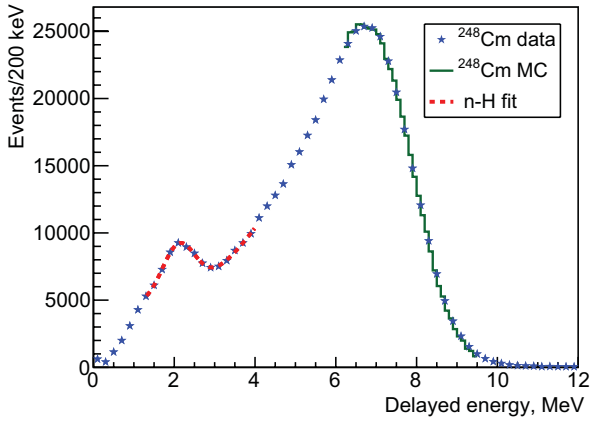

Figure 1. Energy spectrum of the delayed signals measured with the ^{248}Cm neutron source. The dashed curve shows the fit of the n-H peak. The histogram is the MC prediction for the n-Gd peak.

GEANT4 [13] (Version 4.10.4) MC simulation of the detector. The experimental energy resolution for cosmic muon signals in the scintillator strips is 15% worse than that from the MC calculation. Therefore, the additional smearing had been added into MC predictions. More detailed description of detector design can be found in [14].

3. Data taking and analysis

Figure 1 shows the energy distribution of neutron capture signals from a ^{248}Cm source placed at the center of the detector. Two peaks correspond to the neutron capture by protons and by Gd. For the n-H capture the fit (MC) gives the width of 0.49 (0.49) MeV and peak position of 2.04 (1.97) MeV. The MC describes well the high energy part of the n-Gd peak, although there is some tension in the tail. Figure 2a shows the difference between the MC and data divided by the data for the main part of the n-Gd peak. There is a good agreement between the MC and data. On the other hand, the slight changes in the MC energy scale or in the MC energy resolution lead to serious discrepancies between the data and MC (see Fig. 2b and Fig. 2c). This comparison indicates the scale of the systematic uncertainties of these parameters. It is very difficult to simulate reliably the low energy part of the n-Gd capture signal since there are many cascade decay chains with unknown probabilities. Our MC does not describe well the lower energy part of the spectrum and hence we do not use it for the comparison. Figure 3 shows the energy distribution of signals from a ^{60}Co and ^{22}Na γ-sources placed in the center of the detector. The observed energy resolutions and peak positions are consistent with the MC expectations.

The SiPM gain calibration was performed typically every 5 days with noise signals. Calibration with cosmic muons of all strips in the whole detector was also performed once in 5 days. A detailed description of the calibration procedure is presented in [15]. High granularity of the detector allows to reconstruct muons crossing the strips at different angles. Energy deposit inside the strip is proportional to the muon track length in the strip. The accuracy of track reconstruction algorithm was estimated by MC by comparing reconstructed and generated tracks. Figure 4 shows the deviation of the reconstructed length

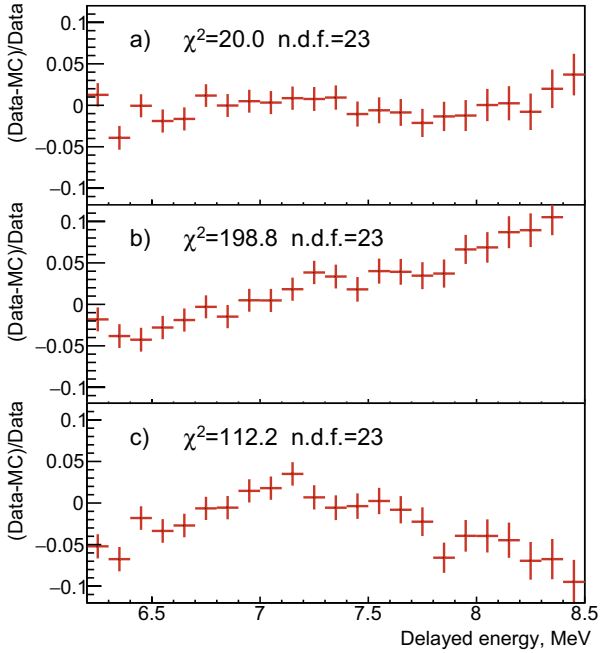

Figure 2. Ratio of the difference in MC predictions and data divided by the data for the neutron capture signal on Gd for: a) Nominal MC parameters; b) The MC energy scale increased by 1%; c) The MC energy resolution worsened by 5% of its nominal value. χ^2 values correspond to the deviations of the points from the zero line.

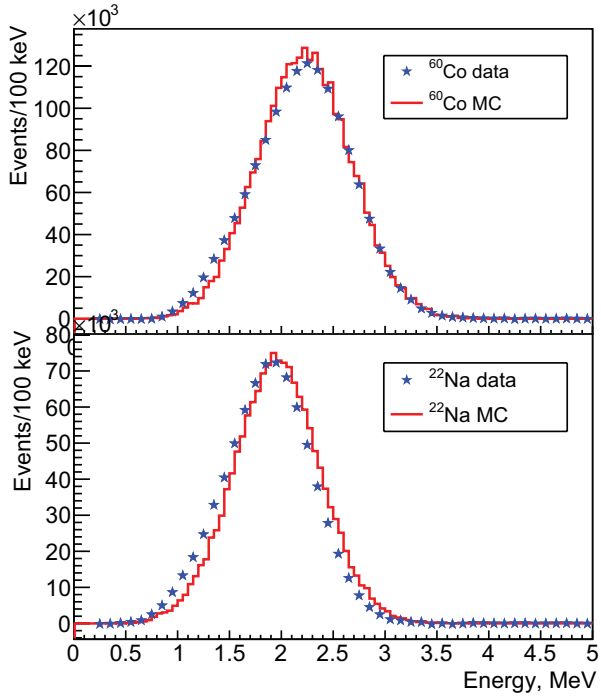

Figure 3. Detector response to the ^{60}Co and ^{22}Na sources. Histograms are the MC predictions.

inside the strip from its generated value. The accuracy is better than 0.5%. After correcting for cross-talk and saturation curve, the strip response to the energy deposited by cosmic muons is linear within 0.7% in the range (1.7–4.7) MeV (Fig. 5). The energy measured with PMTs is proportional on average to the energy, measured with SiPMs. This was checked comparing the positron energy from IBD events reconstructed with SiPMs and with

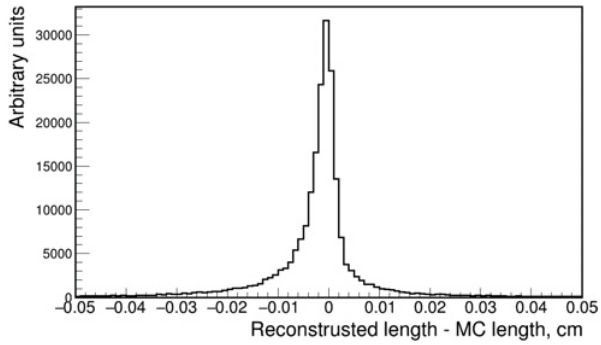

Figure 4. Distribution of track length difference. Typical track length inside a strip is about 1 cm.

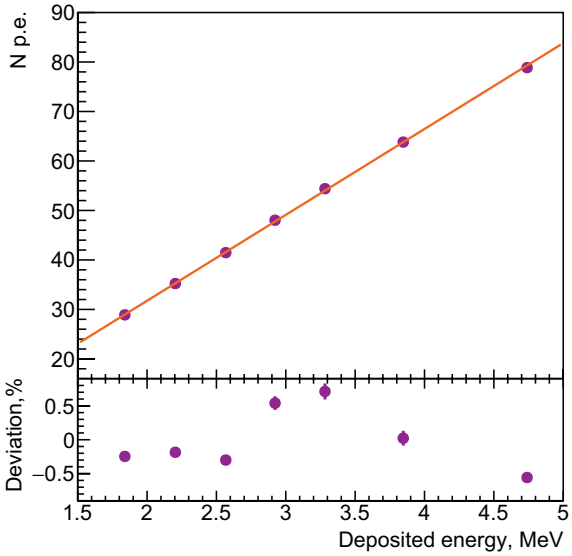

Figure 5. Number of p.e. detected with SiPMs vs energy deposited by cosmic muons in a scintillator strip (top) and the deviation from a straight line fit (bottom). Different muon energies correspond to different crossing angles of the muons and the strips.

PMTs. The PMT linearity was also checked using the LED calibration system. Therefore, the PMT energy response is also linear. Positrons with energies higher than 4.7 MeV typically deposit their energy in several strips. Therefore, the detector response should be linear for high energies as well.

The trigger of the experiment is produced when the digital sum of all PMT signals is above 0.7 MeV or the energy in the veto system is larger than 4 MeV. The IBD process appears in the data as two distinct events, prompt and delayed. For each trigger, waveforms for all SiPMs and PMTs are recorded in 512 ns windows. The visible energy of a positron cluster (continuous cluster of hits in the strips) is converted using MC simulations into the deposited energy by taking into account average losses in the inactive reflective layers of the strips and dead channels. Sometimes photons from the positron annihilation produce signals in the strips attributed to the positron cluster. This leads to an increase of the visible energy. Such a shift is also corrected on average using MC simulations. A typical size of the total correction is ∼2%. The next step is a search for the time-correlated pairs of prompt-delayed events. We start with searching

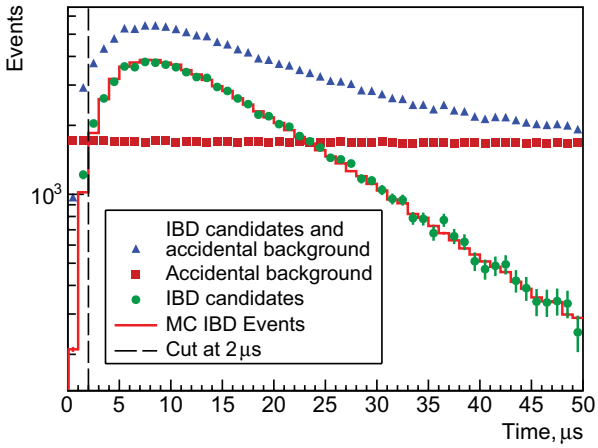

Figure 6. Time between prompt and delayed signals. Errors are smaller than sizes of points.The histogram is the MC prediction for the IBD events.

for an event with more than 3.5 MeV energy deposit. This is a delayed event candidate unless it has the muon veto. Then we look backward in time searching for a prompt event with more than 1 MeV in the positron cluster and no muon veto. An IBD candidate pair is considered found if the time difference between the prompt and delayed events is in the range (2–50) μs. For a valid pair we also require no event with the muon veto within 60 μs before the prompt signal (within 200 μs if E > 300 MeV is released in the main detector). No other event should occur within 45 μs before and 80 μs after the prompt event. The found pairs of prompt and delayed events form the experimental sample of IBD candidates. Similar to the experimental sample, the accidental coincidence sample is formed by looking for a prompt signal in 16 regions: 5, 10,..., 80 ms before the neutron candidate. This sample provides us with a model-independent measure of the accidental background. Distributions for IBD candidates, the accidental background and their difference, which represents the IBD signal without accidental background are presented in Fig. 6.

Several cuts are applied in order to reduce the accidental background. These cuts are designed to be very soft with respect to the signal in order to avoid any distortions. All cuts were selected without looking at the final results. They have been fixed after collection of about 10% of the data. The cuts include the following requirements:

- The distance between positron and neutron candidates should be shorter than 45 cm (55 cm) for a positron candidate reconstructed in 2(3) dimensions;
- The additional energy outside a positron cluster should be less than 1.8 MeV, and the most energetic hit should have the energy less than 0.8 MeV;
- The number of hits in the delayed event is higher than 3;
- The number of hits in the prompt event outside the positron cluster is less than 11;
- The most energetic hit of the positron cluster lies in a fiducial volume of the detector which does not include outer strips in the X and Y directions as well as 4 highest and 4 lowest strips in the vertical

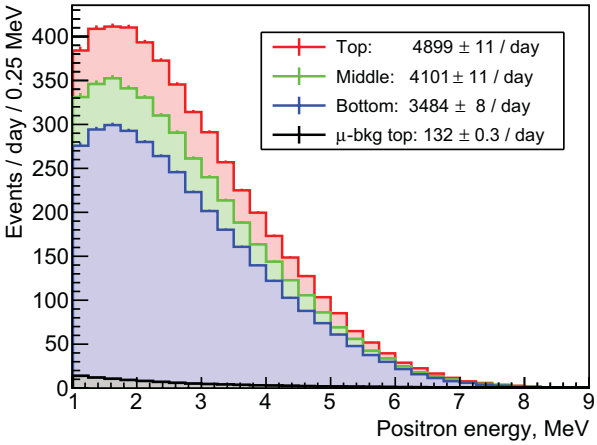

Figure 7. Positron energy distributions measured at different detector positions after subtraction of all backgrounds (statistical errors only). The background from neutrons produced by cosmic muons is shown for the top detector position.

Z direction. This cut excludes regions with fast changes of the efficiency. It is also useful against the background from fast neutrons.

Positron energy spectra for 3 detector positions (top, middle, bottom) are shown in Fig. 7 with statistical errors only. The corresponding numbers of events are 367, 260 and 339 thousand. The IBD counting rate is 4899 events per day in the top position. The positron energy does not include annihilation photons and hence it is 1.02 MeV lower than the usually used prompt energy. The muon-induced background (discussed below) is subtracted. Three other reactors at the KNPP are 160 m, 334 m, and 478 m away from the DANSS detector. The IBD counting rate from these reactors is 0.6% of the IBD counting rate from the nearest reactor for the top detector position. This contribution is taken into account by the corresponding reduction of the normalization of the obtained spectra.

The energy spectrum of the background from neutrons produced by muons inside the veto system is obtained from events with the muon veto. The amount of this background is determined from a fit of the positron candidate energy spectrum during reactor off periods using the shape of the background determined from events with the muon veto. This procedure reduces uncertainties in the background shape to a negligible level. A possible small uncertainty in the background rate is taken into account during systematic error studies. This is the most important background. It constitutes 2.7% of the IBD rate at the top detector position. Rough estimates of the fast neutron penetration probability through the massive reactor shielding indicate that this background is much smaller than 0.1 events/day. In addition, fast neutrons should interact predominantly in the outer region of the detector. Such an increase is observed for neutrons produced by muons inside the detector shielding. On the other hand, no such increase is observed for the IBD candidates. Nevertheless to be safe, the outer 4 cm area of the detector in all 3 dimensions is not included into the data analysis.

The shape of the positron spectrum agrees roughly with the MC predictions based on the $\overline{\nu}_e$ spectrum from [3,16]. However, a quantitative comparison requires additional studies of calibration and systematic errors and improvements in the MC simulation of the detector.

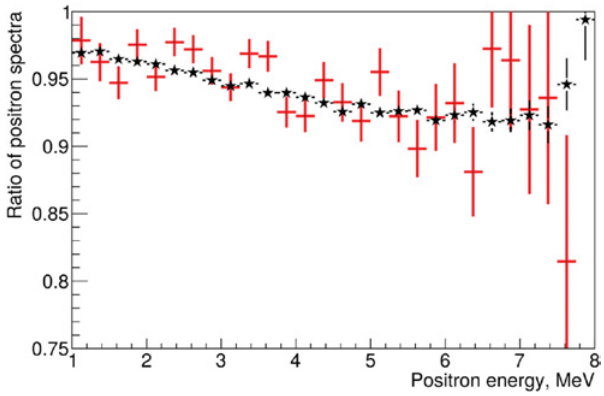

Figure 8. Ratio of positron energy spectra collected during the last 3 months of the reactor campaign in 2017 and during the 2nd–4th months from the beginning of the next campaign (statistical errors only). The average ^{239}Pu fission fractions for these periods are 37.7% and 27.1% correspondingly. Stars are the Hueber-Mueller model MC predictions.

The shapes of the $\overline{\nu}_e$ spectra are different for ^{235}U and ^{239}Pu isotopes. The fractions of these isotopes change during a reactor campaign. The amount of ^{235}U decreases while the amount of ^{239}Pu increases with time. This leads to changes in the $\overline{\nu}_e$ spectrum first observed in [17].

Figure 8 shows the ratio of positron spectra collected during 3 months before the end of the reactor campaign and during the 2–4 months after beginning of the campaign. The corresponding fractions of ^{239}Pu fission fractions are 37.7% and 27.1% correspondingly. We do not have reliable information about the corresponding fraction during the first month after the start of the reactor campaign. The changes in the positron spectrum are obvious. They are well described by the MC expectations based on the $\overline{\nu}_e$ spectra from [3,16]. Figure 9 shows the correlation between the reactor thermal power and the number of registered IBD events. The two distributions were equalized during one month period in 2016. The number of IBD events was corrected for the fuel evolution using the model of the $\overline{\nu}_e$ spectra [3,16]. After that the IBD rate coincides with the reactor power with about 2% accuracy during 16 months. The only exception is the one month period after the latest beginning of the campaign for which we do not have reliable data on the isotope fractions.

Figure 10 shows the ratio of positron energy spectra at the bottom and top detector positions. The exclusion area in the sterile neutrino parameter space was calculated using the Gaussian CL$_s$ method [18] assuming only one type of sterile neutrinos. For a grid of points in the Δm^2_{14}, $\sin^2 2\theta_{14}$ plane predictions for the ratio $R_i^{\rm pre}$ of positron spectra at the bottom and top detector positions were calculated. Calculations included the MC integration over the $\overline{\nu}_e$ production point in the reactor core, $\overline{\nu}_e$ detection point in the detector, and positron energy resolution. The $\overline{\nu}_e$ production point distributions in the reactor core were provided by the KNPP for different time periods. The distribution averaged over the campaign was used in the calculations. It was checked that this approximation practically did not influence the final results. The obtained theoretical prediction for a given point in the Δm^2_{14}, $\sin^2 2\theta_{14}$ plane was compared with the prediction for the three neutrino case using the Gaussian CL$_s$ method for the 90% confidence level

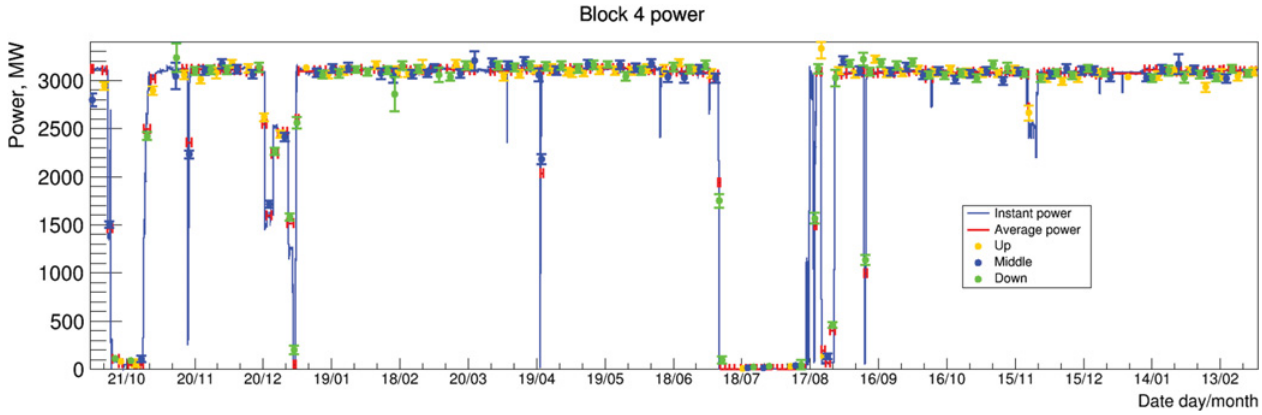

Figure 9. IBD counting rate at different detector positions (points) and the reactor thermal power. The distributions are equalized during the period November-December 2016 and therefore the IBD rate is expressed in MW. The IBD rate is corrected for the fuel evolution with time using Huber-Mueller model. Statistical errors only.

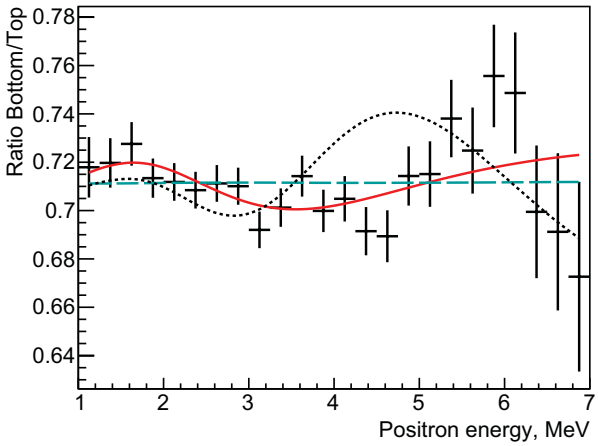

Figure 10. Ratio of positron energy spectra measured at the bottom and top detector positions (statistical errors only). The dashed curve is the prediction for 3ν case ($\chi^2 = 35.0$, 24 degrees of freedom). The solid curve corresponds to the best fit in the 4ν mixing scenario ($\chi^2 = 21.9$, $\sin^2 2\theta_{14} = 0.05$, $\Delta m^2_{14} = 1.4\ \mathrm{eV}^2$). The dotted curve is the expectation for the optimum point from the RAA and GA fit [4] ($\chi^2 = 83$, $\sin^2 2\theta_{14} = 0.14$, $\Delta m^2_{14} = 2.3\ \mathrm{eV}^2$).

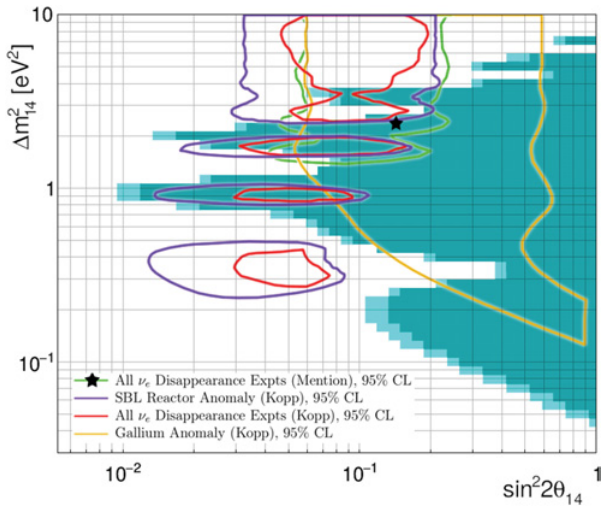

Figure 11. 90% (light cyan) and 95% (dark cyan) CL exclusion area in Δm^2_{14}, $\sin^2 2\theta_{14}$ parameter space. The shaded area represents our analysis. Curves show allowed regions from neutrino disappearance experiments [4,21], and the star is the best point from the RAA and GA fit [4].

(CL) exclusion area estimation. The difference in χ^2 for the two hypotheses $\Delta\chi^2 = \chi^2_{4\nu} - \chi^2_{3\nu}$ was used for the comparison. The χ^2 for each hypothesis was constructed using 24 data points R_i^{obs} in the (1−7) MeV positron energy range

$$\chi^2 = \sum_{i=1}^{N} (R_i^{\mathrm{obs}} - k \times R_i^{\mathrm{pre}})^2 / \sigma_i^2, \qquad (3)$$

where R_i^{obs} (R_i^{pre}) is the observed (predicted) ratio of $\overline{\nu}_e$ counting rates at the two detector positions and σ_i is the statistical standard deviation of R_i^{obs}, and k is a normalization factor equal to the ratio of the total number of the IBD events per day at the bottom and top detector positions (MC events number were equal for different positions). The oscillations due to the known neutrinos were neglected since at such short distances they do not change the $\overline{\nu}_e$ spectrum. The procedure was repeated for all points of the grid in order to get the whole exclusion area. Influence of systematic uncertainties in the parameters was estimated by repeating the analysis with different values of parameters. A point in the Δm^2_{14}, $\sin^2 2\theta_{14}$ plane was included into the final exclusion area if it appeared in the exclusion areas for all tested variations of the parameters. We varied the energy resolution, the background level and energy scale by 10%, 15% and 2% correspondingly. We also used a reduced energy range of (1.5−6) MeV in the fit.

Figure 11 shows the obtained 90% and 95% CL excluded area in the Δm^2_{14}, $\sin^2 2\theta_{14}$ plane. For some values of Δm^2_{14} the obtained limits are more stringent than previous results [6,19,20]. It is important to stress that our results are based only on the comparison of the positron energy distributions at the two distances measured with the same detector. Therefore the results do not depend on the $\overline{\nu}_e$ spectrum shape and normalization as well as on the detector efficiency. The method used in our analysis is very insensitive to systematic errors since the influence of the errors is canceled out in the ratio of the positron spectra at the two distances. This is illustrated by Fig. 12. It shows that the excluded areas with and without the systematic

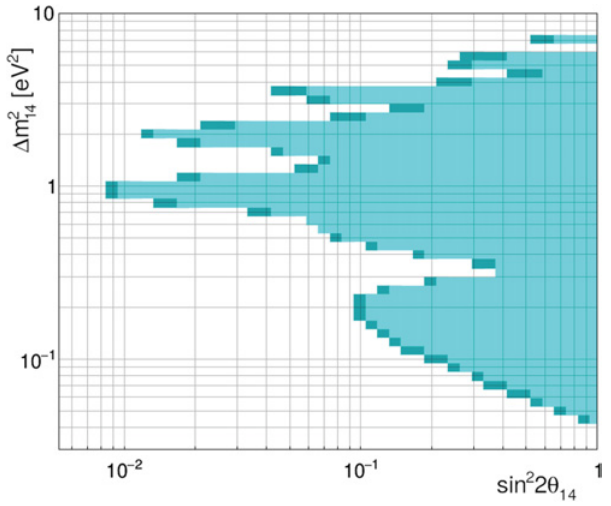

Figure 12. 90% CL exclusion areas in Δm^2_{14}, $\sin^2 2\theta_{14}$ parameter space without systematic uncertainties (dark cyan) and with systematic uncertainties (light cyan).

errors differ very little. The excluded area covers a large fraction of regions indicated by the GA and RAA. In our analysis the point $\Delta m^2_{14} = 1.4\text{eV}^2$, $\sin^2 2\theta_{14} = 0.05$ has the smallest $\chi^2 = 21.9$. The difference in χ^2 with the 3ν case is 13.1. The significance of this indication of the existence of the sterile neutrino will be studied taking into account systematic uncertainties after collection of more data this year.

The authors are grateful to the directorates of ITEP and JINR for constant support of this work. The authors appreciate the permanent assistance of the KNPP administration and Radiation and Nuclear Safety Departments. The detector construction was supported by the Russian State Corporation ROSATOM (state contracts H.4x.44.90.13.1119 and H.4x.44.9B.16.1006). The operation and data analysis became possible due to the valuable support from the Russian Science Foundation grant 17-12-01145.

References

[1] The ALEPH Collaboration, The DELPHI Collaboration, The L3 Collaboration, The OPAL Collaboration, The SLD Collaboration, The LEP Electroweak Working Group, The SLD Electroweak and Heavy Flavour Groups, Phys. Rep. **427**, 257454 (2006)
[2] J.N. Abdurashitov et al., Phys. Rev. C **73**, 045805 (2006)
[3] T.A. Mueller et al., Phys. Rev. C **83**, 054615 (2011)
[4] G. Mention et al., Phys. Rev. D **83**, 073006 (2011)
[5] I. Alekseev et al., Phys. Lett. B **787**, 56 (2018)
[6] Y.J. Ko et al., Phys. Rev. Lett. **118**, 121802 (2017)
[7] A.P. Serebrov et al., JETP Lett. **109**(4), 213–221 (2019)
[8] A.P. Serebrov et al., JPCS **798**, 012116 (2017)
[9] J. Ashenfelter et al., Phys. Rev. Lett. **121**, 251802 (2018)
[10] N.V. Remortel, Talk at XXVIII International Conference on Neutrino Physics and Astrophysics, 4-9 June 2018, Heidelberg, Germany (2018)
[11] Y. Abreu et al., JINST **12**, P04024 (2017)
[12] H. Almazan et al., Phys. Rev. Lett. **121**, 161801 (2018)
[13] S. Agostinelli et al., Nucl. Instrum. Meth. A **506**, 250 (2003)
[14] I. Alekseev et al., JINST **11**, P11011 (2016)
[15] I. Alekseev et al., Lett. Elem. Part. Atom. Nucl. **15**, 272 (2018)
[16] P. Huber, Phys. Rev. C **84**, 024617 (2011)
[17] Y. Klimov, V. Kopeikin, L. Mikaelyan, K. Ozerov, V. Sinev, Atomic Energy **76**, 123 (1994)
[18] X. Qian et al., Nucl. Inst. Meth. A **827**, 63 (2016)
[19] B. Achkar et al., Nucl. Phys. B **434**, 503 (1995)
[20] P. Adamson et al., Phys. Rev. Lett. **117**, 151801 (2016)
[21] J. Kopp, P.A.N. Machado, M. Maltoni, T. Schwetz, JHEP **1305**, 050 (2013)